PCCP

Nuclear Quantum Effects on the Liquid-Liquid Phase Transition of a Water-Like Monatomic Liquid

Journal:	*Physical Chemistry Chemical Physics*
Manuscript ID	CP-ART-12-2017-008505.R1
Article Type:	Paper
Date Submitted by the Author:	23-Feb-2018
Complete List of Authors:	NGUYEN, BINH ; Lehman College of the City University of New York, Chemistry Lopez, Gustavo; Lehman College of the City University of New York, Chemistry Giovambattista, Nicolas; CUNY, Brooklyn College

Nuclear Quantum Effects on the Liquid-Liquid Phase Transition of a Water-Like Monatomic Liquid

Binh Nguyen[1], Gustavo E. Lopez[1,2*], and Nicolas Giovambattista[2,3,4**]

[1] *Department of Chemistry, Lehman College of the City University of New York, Bronx, New York 10468, United States*

[2] *Ph.D. Program in Chemistry, The Graduate Center of the City University of New York, New York, NY 10016*

[3] *Department of Physics, Brooklyn College of the City University of New York, Brooklyn, New York 11210, United States*

[4] *Ph.D. Program in Physics, The Graduate Center of the City University of New York, New York, NY 10016*

E-mail: gustavo.lopez1@lehman.cuny.edu,ngiovambattista@brooklyn.cuny.edu

Abstract

Polymorphic substances have the ability to exist in more than one liquid and/or glass states. Examples include water, silicon, and hydrogen. In many of these substances, nuclear quantum effects may become important in the proximity of the liquid-liquid and glass-glass transformation. Here, we study the nuclear quantum effects on a monatomic liquid that exhibits water-like anomalous properties and a liquid-liquid phase transition (LLPT) ending at a liquid-liquid critical point (LLCP). By performing path integral Monte Carlo simulations with different values of the Planck's constant h, we are able to explore how the location of the LLCP/LLPT in the P-T plane shifts

as the system evolves from classical, $h = 0$, to quantum, $h > 0$. We find that, as the quantum nature of the liquid (as quantified by h) increases, and the atoms in the liquid become more delocalized, the LLCP pressure increases, the LLCP temperature decreases, and the LLCP volume remains constant. In addition, the crystallization temperature decreases with increasing h. For large values of h, the LLCP is not accessible due to rapid crystallization. The structure of the liquids studied at different values of h are also investigated.

1 Introduction

A common P-T phase diagram proposed for polymorphic liquids, such as silicon and water[1–9] consists of two liquid states, low- and high-density liquids (LDL and HDL), separated by a first-order liquid-liquid phase transition (LLPT) ending at a liquid-liquid critical point (LLCP) (at high-temperature and either positive or negative pressures); see, e.g, Refs.[10–14] In this scenario, the LLPT line at *low* temperature ends at the melting line (see, e.g., Ref.[15]) or, if crystallization can be avoided, it extends into the glass state, giving origin to two amorphous solids, low- and high-density amorphs (LDA and HDA). Indeed, the strongest evidence of liquid polymorphism is usually from experiments in the glass state where a sharp, first-order-like phase transitions between LDA and HDA forms is observed (see, e.g., Refs.[9,11,16,17]).

Computer simulations of polymorphic liquids are usually based on classical models or combine classical and first principles techniques with *nuclear* quantum effects being neglected. Molecular liquids such as water fall in the first group since for these systems, relaxation times in the proximity of the LLCP/LLCP are large and first principle computer simulations require inaccessible computational resources. We note that the LLCP in water is estimated to be located at approximately $P_c = 50$ MPa and $T_c = 223$ K[18] where classical effects may be expected to be dominant. In other polymorphic liquids the LLCP is predicted to exist at high temperatures and low pressures and hence, omission of nuclear quantum ef-

fects may be justified. This is the case of silicon where the hypothesized LLCP is located at $T_c > 1100$ K and negative pressures.[4–6,19] However, for some of these substances, there are situations where quantum effects in the proximity of the LLPT may become relevant. For example, the hypothesized LLPT in water extends at low temperatures to $T \approx 130 - 140$ K (under pressure), close to water's glass transition. At these temperatures, quantum effects are known to occur, as evidenced by the higher glass transition temperature of D_2O relative to H_2O at 1 atm, $\Delta T_g \approx 10$ K.[20,21] Indeed, since water is an unusually light molecule, quantum effects can also be observed at normal temperatures (see, e.g., Ref.[22]); for example, near ambient temperature the difference in structure between H_2O and D_2O corresponds to a shift in temperature by $5 - 10$ K.[23–25] In particular, we note that experiments on H_2O and D_2O are consistent with the presence of a LLPT but provide slightly different locations for the LLPT.[26,27]

The case of hydrogen is particularly interesting. Experiments show the existence of a LLPT at high pressure[28,29] and computer simulations indicate that the LLCP in H_2 is located somewhere in the range of $T_c \approx 1500 - 2000$ K and $P \approx 100 - 200$ GPa.[15,30–33] Since H is the lightest element on Earth, computer simulations in the proximity of the LLPT/LLCP require quantum techniques. Unfortunately, the LLCP location varies with the numerical methods employed. In particular, it has been found that *nuclear* quantum effects shift the LLPT/LLCP pressure considerably, by ≈ 50 GPa relative to computer simulations employing classical protons.[34]

In this work, motivated by the cases of water and hydrogen, we explore the effects of adding *nuclear* quantum effects on the LLPT/LLCP of a classical, monatomic water-like model liquid. This is a classical coarse-grained model of water that is able to reproduce many of water's anomalous properties (e.g., the presence of density maximum upon isobaric cooling and maximum diffusivity upon isothermal compression) and exhibits a LLPT with an associated LLCP; this model also exhibits glass polymorphism, as found in real water. The model is combined with path integral Monte Carlo (PIMC) simulations[35] in order to

include nuclear quantum effects (i.e., delocalization of the liquid atoms). We perform PIMC simulations with different values of Planck's constant, h. This procedure generates a family of polymorphic model liquids, expanding from classical ($h = 0$) to quantum ($h > 0$) in nature, all characterized by the same pair potential interaction. Our focus is to determine (i) how the location of the LLPT/LLCP in the P-T phase diagram evolves as the quantum nature of the liquid increases (or equivalently, as the atoms of the liquid become more delocalized); and (ii) to understand the relationship between the LLPT/LLCP and the structural properties of *polymorphic quantum* liquids.

2 Computer Simulation Details

PIMC simulations are performed for a system of atoms with isotropic pair-interactions given by the Fermi-Jagla (FJ) potential.[36] This is a core-softened potential characterized by a hard-core radius $r = a$ and an attractive minimum at $r = b \approx 2a$; see Fig. 1(a). In the classical case, where atoms are represented by point particles, the FJ liquid exhibits many of water anomalous properties,[12] including the increase of compressibility and the presence of density maximum upon isobaric cooling, and the existence of a diffusivity maximum upon isothermal compression.[36,37] In particular, this water-like model exhibits a LLPT and LLCP, consistent with computer simulations of several full-atomistic, classical water models.[8,38–44] In the glass state, the model exhibits glass polymorphism with sharp transformations between a low-density and a high-density amorphous solids (LDA and HDA).[45,46] The LDA-HDA transformation in the FJ model is reminiscent of first-order phase transitions in equilibrium systems, which is also the case of the LDA-HDA transformation in (real) water.[9]

We employ the path integral formulation of statistical mechanics (see, e.g., Ref.[35]) to study the quantum analog of the classical FJ liquid defined in Ref.[36] In this formulation, the canonical partition function of the *quantum* liquid is shown to be isomorphic to the canonical partition function of a *classical* liquid composed of ring polymers. Specifically,

in the quantum case, each atom of the classical liquid is replaced by a ring polymer of n_b beads where the beads are connected by springs with spring constant $K_{sp} = 2\pi n_b/(\beta\lambda^2)$, where $\lambda = h/\sqrt{2\pi m k_B T}$ is de Broglie's thermal wavelength, $\beta = 1/k_B T$, and m is the mass of the atoms. The ring polymers interact via pair interactions that are rather peculiar: bead n_1 ($n_1 = 1, 2, ..., n_b$) of a given ring polymer interacts with bead n_2 ($n_2 = 1, 2, ..., n_b$) of neighboring ring polymers *only if* $n_1 = n_2$; otherwise, beads do not exert forces on one another. In the case $n_1 = n_2$, the bead-bead pair interactions are given by the same pair interaction potential defined between atoms in the classical liquid but rescaled by a factor $1/n_b$. For example, in the present study, the bead-bead interactions are given by the FJ potential shown in Fig. 1(a) (rescaled by a factor $1/n_b$) where r is the bead-bead distance.

In the present work, we study the LLPT/LLCP using PIMC simulations of a family of FJ liquids, each liquid differing by the value of h in the expression of K_{sp}. This allows us to study how the location of the LLPT/LLCP in the P-T plane shifts as h increases ($h \geq 0$), i.e., as the quantum character of the liquid is enhanced. The case $h = 0$ is the classical limit since it leads to $K_{sp} = \infty$, which implies that all beads are forced to collapse to a single point. Accordingly, the ring polymers become effectively point particles with inter-particle interactions given by the FJ pair potential. As h increases, K_{sp} decreases allowing the bead-bead distance to increase (at a given T and V) and hence, the atoms in the liquid become more delocalized.

All PIMC simulations are performed for a system of $N = 1000$ atoms, each atom represented by $n_b = 10$ beads, at constant temperature and volume. In one MC step, we first move all the 10000 beads and then, the centroids of all N ring polymers are displaced. The system is equilibrated for 10^6 MC steps and simulations are run for at least 10^6 additional MC steps for data analysis. After equilibration, we also save configurations of the system every 1000 MC steps to study the structure of the liquid. We confirm that the system is equilibrated by monitoring the decay, with the number of MC step, of thermodynamic properties such as energy and pressure as well as the correlation function of the beads and centroids position.

We also perform PIMC simulations at selected (V,T) states using $n_b = 20$ and confirm that our results are not sensitive to the number of beads per particle considered. We note that for the case $h \to 0$, we recover the location of the LLCP for the classical FJ liquid reported in Ref.,[36] $P_c \approx 0.35$, $T_c \approx 0.18$ and $v_c = V_c/N \approx 2.9$ in reduced units. Reduced units are defined by setting the particle mass $m = 1$ and the Boltzmann constant $k_B = 1$; energies and distances are given in units of ϵ_0 and a, respectively; see also Ref.[36] It follows that the units of h are $a\ \epsilon_0^{1/2}$.

3 Results

Simulations are performed at the values of (h, T) indicated in Fig. 1(b). For each point in Fig. 1(b), we perform runs at $v = V/N = 2.0,\ 2.2,\ 2.4...4.0$ in order to construct the $P(v)$ isotherm at a given (h, T). Simulations are performed along constant-h and constant-λ paths. Simulations performed at constant h show the effects of T on the quantum FJ liquid when the quantumness of the physical laws are fixed, i.e., in this case, the same Schrödinger equation determines the evolution of the system at all T. Instead, for simulations at constant λ, h decreases with decreasing T and hence, the quantumness of the physical laws, as quantified by h, decreases upon cooling. It follows that, from the physical point of view, only simulations at constant h are meaningful. Nonetheless, simulations at constant λ are relevant since λ indicates the length-scale at which wave-like phenomena, such as diffraction, are expected to occur (see, e.g., Ref.[47]). Accordingly, one may consider that simulations at constant λ show the T-effects on the quantum FJ liquid as the wave-like character of the atoms is preserved. From a practical perspective, constant-λ simulations allow us to explore efficiently the $h - T$ plane of Fig. 1(b).

3.1 Location of the LLPT/LLCP in the P-T Plane

In order to determine the LLCP pressure, temperature, and volume along a constant-h or constant-λ path in Fig. 1(b) we focus on the corresponding $P(v)$-isotherms as function of T. In this work we consider the cases $h = h_1,\ h_2$, and h_3 where $h_1 = 0.2474$, $h_2 = 0.5150$, and $h_3 = 0.7948$; h_3 is the largest value of h for which crystallization occurs at $T < T_c$. We also consider the cases $\lambda = 0.0251,\ 0.2507,\ 0.4512,\ 0.6267,\ 1.0026,\ 1.2533,\ 1.3786,\ 1.8800,\ 2.5066$. As an example, we include in Figs. 2(a)-(c) the $P(v)$-isotherms for $h = h_1$, $\lambda = 0.2507$, and $h = h_3$. We note that our $P(v)$-isotherms for the quantum FJ liquids at $h \to 0$ are in agreement with the $P(v)$-isotherms of the classical liquid shown in Fig. 3 of Ref.[36] For all values of h considered, and in agreement with the thermodynamics of first-order phase transitions, we find that at $T > T_c$, the $P(v)$-isotherms are monotonic decaying functions of v while at $T < T_c$, the $P(v)$-isotherms exhibit van der Waals loops. At $T = T_c$, the $P(v)$-isotherm exhibits an inflexion point. The same qualitative behavior of the $P(v)$-isotherms is found along constant-λ paths; see, e.g., Fig. 2(b).

Included in Fig. 1(b) is the location of the LLCP temperature as function of h (red dashed line). As $h \to 0$, we obtain the classical value $T_c \to 0.18$ reported in Ref.,[36] while in the opposite limit, $h \to h_3$, we find that $T_c \to 0.06$. This is a rather small value, i.e., $T_c(h = h_3) \approx T_c(h = 0)/3$. In particular, $T_c(h = h_3)$ is much smaller than the crystallization temperature of the classical liquid $T_x(h = 0) \approx 0.14 - 0.16$ for $v_c < v < 4.0$, i.e., at the volumes where crystallization is favored.[36] It follows that crystallization is also suppressed as h increases. This is shown in Fig. 1(b) where $T_x(h)$ is included for the quantum FJ liquids at $v < 3.0 - 3.2$, just above v_c. The crystallization temperature in Fig. 1(b) (black dashed-line) decreases with increasing h and intersects the LLCP temperature line at $h \approx h_3$.

We note that the level of quantumness of the FJ liquids studied is not negligible. To show this, we compare the value of λ explored here, $\lambda \approx 0 - 2.5$ (in reduced units of a), with the corresponding value for the case of H_2 at the hypothesized LLCP temperature $T_c \approx 2000$ K ($P_c \approx 120$ GPa) from Ref.[48] Specifically, for H_2, $m = 2 \times 1.008$ g/mol and $T = T_c \approx 2000$ K

and hence, $\lambda = h/\sqrt{2\pi m k_B T} = 0.0275$ nm. If one considers that a is approximately the location of the first maximum of the radial distribution function ≈ 0.074 nm[34] then $\lambda \approx 0.37$ in reduced units, which is within the range of λ values explored in this work. A similar comparison can be made for the case of water. In this case, we consider $T = T_g = 136$ K, where T_g is the glass transition of water at $P = 1$ atm, since quantum effects are observed at this temperature in experiments of H_2O and D_2O (see, e.g., Ref.[20]). As explained in Ref.,[49] Jagla-like potentials can be thought to be coarse-grained models of water where one particle corresponds to $1 + 4 \times 1/4 = 2$ water molecules. Accordingly, for comparison with water, we consider $m = 2 \times 18.016$ g/mol. Since $a \approx 0.28$ nm is the location of the first peak of the RDF of water, it follows that $\lambda = 0.09$ in reduced units. Again, this is within the range of values for λ considered in this work.

The evolution of the LLCP/LLPT with increasing h is shown in Figs. 3(a)-(c). For $h \to 0$, we recover the values of ($P_c = 0.35,\ T_c = 0.18,\ v_c = 2.9$) reported in Ref.[36] for the classical FJ liquid. With increasing h, i.e., as the FJ liquid becomes increasingly quantum, P_c increases while T_c decreases. Interestingly, the critical volume is invariant to the degree of quantumness of the liquid, $v_c \approx 2.9$. For approximately $h > h_3$, the LLCP is not accessible due to rapid crystallization. For comparison, we include in the insets of Fig. 3(a)-(c) the behavior of ($P_c,\ T_c,\ v_c$) as function of λ.

3.2 Structural Properties

We also describe the structure of the quantum FJ liquids obtained at different values of h and λ. We focus on the case $T = T_c(h)$ and $h = h_1,\ h_2,\ h_3$; at $T = T_c(h)$ these values of h correspond to $\lambda = 0.2507,\ 0.6267,\ 1.2533$, respectively [see Fig. 1(b)]. To characterize the structure of the liquids, we consider the (i) bead-bead and centroid-centroid radial distribution functions (RDFs) and the (ii) local orientational order parameter Q_6 and translational order parameter t_p defined in Refs.[50,51] We follow a similar analysis to that presented in Refs.[36,45] for the classical FJ liquid and glass. Once again, our results for $h \to 0$

are consistent with the results of Ref.[45] and hence, we focus on the opposite limit, $h = h_3$.

Fig. 4(a) shows the centroid-centroid RDF $g_{cc}(r)$ at $h = h_3$ and $T = T_c$. The effect of volume on the structure of the quantum FJ liquids is analogous to the structural changes found in the classical FJ liquid.[45] Specifically, in the LDL-like liquid (e.g., $v = 3.2$), the RDF exhibits a large first peak at $r \approx 1.7$, corresponding to particles located at approximately the minimum of the FJ potential [Fig. 1(a)]. At small volumes, in the HDL-like state (e.g., $v = 2.0$), the $g_{cc}(r)$ exhibits an extra peak at $r \approx 1$, i.e., at the hard-core distance of the FJ potential. Accordingly, the effect of reducing v is to move particle centroids from the minimum of the FJ potential ($r = 1.7 \approx b$) to the hard-core repulsive part of the FJ potential ($r = 1.0$). Interestingly, the same structural qualitative changes occur at the level of the ring polymer beads. This follows from Fig. 4(b) which shows the RDF between the n-th bead of a given polymer and the m-bead of neighbor polymers for the case $m = n$ (i.e., interacting beads). The inset of Fig. 4(b) shows the bead-bead RDF for the case where all beads of all polymers are considered. Since non-interacting beads (of a given ring polymer or from different ring polymers) can overlap, the bead-bead RDF in the inset of Fig. 4(b) is non-zero for $r \approx 0$.

We stress that the quantum character of the liquid is not negligible, i.e., the beads of the ring polymers associated to the atoms of the liquid are indeed displaced from the corresponding centroids. This follows from the inset of Fig. 4(a) that shows the probability $P_{bc}(r)$ to find a bead of a ring-polymer (atom) at a distance r from the corresponding centroid, at $T = T_c$. At this temperature (and for $h = h_3$), beads can move up to approximately $0.4 \times a$, or 40% the hard-core radius of the FJ pair potential. Not surprisingly, reducing the quantum character of the liquid leads to an increasing localization of the ring polymer beads. For example, the maximum bead-centroid distance decreases from 0.4 to only 0.1 as h decreases from h_3 to h_1; see Fig. 5. The radius of gyration R_g of the ring polymers at all volumes and h studied are shown in the inset of Fig. 5(g). Interestingly, for all FJ liquids considered, the 'size' of the atoms is roughly constant with v and depends mostly

on the liquid quantumness (h). It follows that the atom size does not depend on whether the system is in the LDL or HDL state. We note that for the most quantum of the FJ liquids studied ($h = h_3$), a weak maximum occurs in $R_g(v)$. Such a maximum is located in the proximity of the LLCP and hence, it may be related with the presence of maximum in density fluctuations that are known to exist at $v \approx v_c$ and $T \approx T_c$ (see, e.g, Refs.[14,52]).

Complementary analysis of the liquid structure based on the local orientational order parameter Q_6 defined in Ref.[50] and translational order parameter t_p defined in Ref.[51] is provided in the Supplementary Material (SM). We employ these parameters to discriminate efficiently the presence of crystallization.

3.3 Potential of Mean Force

It may be rather unexpected that quantum FJ liquids for $h \approx h_3$ can exhibit a LLCP given that the associated ring polymers (atoms) are very different in nature (see, e.g., Fig. 5). After all, in the case of the classical FJ liquid, the LLPT/LLCP usually disappear rapidly when small perturbations, such as confining surfaces, are included.[53] Similarly, minor modification of atomistic pair potentials that exhibit LLPT/LLCP tend to suppress the LLPT/LLCP.[54–56]

In order to get insight into the origin of the LLCP in the FJ quantum liquids for $h \leq h_3$, we compare the $g_{cc}(r)$ and centroid-centroid potential of mean force (PMF) $W_{cc}(r)$ of the quantum FJ liquids at equivalent conditions, $v = 3.4$ (LDL) and $v = 2.4$ (HDL), and for $T = T_c(h)$; see Fig. 6. The PMF is defined as $W_{cc}(r) = -k_B T \ln[g_{cc}(r)]$.[57] The main point of Fig. 6 is that for both LDL and HDL, the relative spatial arrangements of the atoms centroids is rather independent of the quantum level of the liquid (h). In other words, the effect of increasing h is to decrease T_c and to change the effective interactions between atoms (PMF), while maintaining $g_{cc}(r)$ practically unaffected. This suggests that the LLCP/LLPT are uniquely defined by the structure of the quantum liquid, i.e., by the centroid-centroid RDF. This is consistent with the relationship between structure and thermodynamics in *classical* atomic liquids (with pair interactions), where thermodynamic properties, such as

the pressure- and energy-equation of state, can be expressed in terms of the corresponding RDF.[57,58]

3.4 Summary and Discussion

The aim of this work was to study the *nuclear* quantum effects on the LLPT/LLCP of polymorphic liquids. To do this, we performed PIMC simulations of the FJ liquid, a monatomic water-like model liquid that exhibits liquid and glass polymorphism. PIMC simulations were performed with different values of Planck's constant, allowing us to study the effects of delocalization of the atoms in the liquid. In the case $h = 0$, we reproduced the results obtained previously for the *classical* FJ liquid. With increasing h, and as the nature of the liquid becomes more quantum, it was found that (i) the LLCP pressure P_c increases and (ii) the LLCP temperature T_c decreases, while (iii) the LLCP volume remains constant; (iv) the crystallization temperature line $T_m(P)$ in the P-T plane moves towards lower temperatures; and (v) at very large values of h, the LLCP/LLPT become inaccessible due to unavoidable crystallization.

Not surprisingly, the structure of the liquids studied at given (v, T) state varies with the quantum nature of the liquid, as quantified by h. Accordingly, the potential of mean force extracted from the centroid-centroid RDF also varies with increasing h, i.e., as the atoms become more delocalized. However, for all quantum liquids studied, the structure of LDL and HDL states *at the corresponding* $T_c(h)$ remains unchanged. This suggest that, it is the structure of the quantum liquid, defined by the ring-polymer (atom) centroids, what determines the liquid's phase behavior. Interestingly, in the case of *classical* monatomic liquids with pair-interactions one can show that thermodynamic properties, such as pressure, can be obtained solely from the liquid's structure (see, e.g.,[57]).

Quantum effects are known to occur in water. While a direct comparison of our results and real water should be taken with caution, we note that points (i), (ii), and (iv) are consistent with experiments in H_2O and D_2O. Specifically, points (ii) and (iv) sug-

gest that T_m and T_c should be lower for H_2O than for D_2O since quantum effects increase if $D_2O \rightarrow H_2O$. Similarly, point (i) implies that P_c should be higher for H_2O than for D_2O. Indeed, experiments indicate that $T_m^{H_2O} - T_m^{D_2O} \approx -3$ K[27] and rough estimations of the LLCP based on decompression-induced melting of high-pressure ices[26,27] indicate that $T_c^{H_2O} - T_c^{D_2O} \approx -6 \pm 2$ K, and $P_c^{H_2O} - P_c^{D_2O} \approx 50 \pm 30$ MPa. Comparison with H_2 is less straightforward since experimental data of H_2 in the proximity of the estimated LLCP is not easily accessible. Quantum computer simulations of H_2[15,34] suggest that nuclear quantum effects tend to reduce P_c and leave T_c practically unchanged, which is different from the results found with the FJ quantum liquids. However, the location of the LLCP in H_2 is sensitive to the treatment of *both* the electrons and the nucleus;[34] in the case of H_2, numerical methods are very sensitive to the functional employed in the corresponding density functional calculations.[34]

Acknowledgments

This work was supported, in part, by a grant of computer time from the City University of New York High Performance Computing Center under NSF Grants CNS-0855217, CNS-0958379 and ALI-1126113. GEL acknowledges support from the NSF CREST Center for Interface Design and Engineered Assembly of Low Dimensional systems (IDEALS), NSF grant number HRD-1547830. NG acknowledges support from NSF, Grant No. 1604504.

References

(1) H. E. Stanley (editor). *Liquid Polymorphism*; Advances in Chemical Physics, vol. 120, John Wiley & Sons, Inc., Hoboken, 2013.

(2) L. I. Aptekar, *Sov. Phys. Dokl.*, 1979, **24**, 993-995.

(3) S. Sastry and C. A. Angell, *Nature Mater.*, 2003,**2**, 739-743.

(4) V. V. Vasisht, S. Saw, and S. Sastry, *Nature Mat.*, 2011, **7**, 549-553.

(5) P. Ganesh and M. Widom, *Phys. Rev. Lett.*, 2009, **102**, 075701.

(6) N. Jakse and A. Pasturel, *Phys. Rev. Lett.* **99**, 2007, 205702.

(7) M. Beye, F. Sorgenfrei, W. F. Schlotter, W. Wurth, and A. Föhlich, *Proc. Natl. Acad. Sci. USA*, 2010, **107**, 16772-16776.

(8) P. H. Poole, F. Sciortino, U. Essmann, and H. E. Stanley, *Nature*, 1992, **360**, 324-328.

(9) O. Mishima, and H. E. Stanley, *Nature*, 1998, **396**, 329-335.

(10) P. G. Debenedetti, and H. E. Stanley, *Phys. Today*, 2003, **56**, 40-46.

(11) P. G. Debenedetti, *J. Phys.: Condens. Matter*, 2003, **15**, R1669-R1726.

(12) P. Gallo, K. Amann-Winkel, C. A. Angell, M. A. Anisimov, F. Caupin, C. Chakravarty, E. Lascaris, T. Loerting, A. Z. Panagiotopoulos, J. Russo, J. A. Sellberg, H. E. Stanley, H. Tanaka, C. Vega, L. Xu, and L. G. Pettersson, *Chem Rev.*, 2016, **116**, 7463-7500.

(13) P. F. McMillan, *J . Mater. Chem.*, 2004, **14**, 1506-1512.

(14) N. Giovambattista, The Liquid-Liquid Phase Transition, Anomalous Properties, and Glass Behavior of Polymorphic Liquids, in *Liquid Polymorphism*, Volume **152**, ed. H. E. Stanley, (John Wiley & Sons, Inc., Hoboken, 2013).

(15) M. Morales, C. Pierleoni, E. Schwegler, and D. M. Ceperley, *Proc. Natl. Acad. Sci. USA*, 2010, **107**, 12799-12803.

(16) T. Loerting and N. Giovambattista, *J. Phys.: Condens. Matter*, 2006, **18**, R919-R977.

(17) P. F. McMillan, M. Wilson, M. C. Wilding, D. Daisenberger, M. Mezouar, and G. N. Greaves, *J. Phys.: Condens. Matter*, 2007, **19** 415101.

(18) O. Mishima, *Proc. Jpn. Acad., Ser. B*, 2010, **86**, 165-175.

(19) G. Zhao, Y. J. Yu, J. L. Yan, M. C. Ding, X. G. Zhao, and H. G. Wang, *Phys. Rev. B*, 2016, **93**, 140203(R).

(20) C. Gainaru, A. L. Agapov, V. Fuentes-Landete, K. Amann-Winkel, H. Nelson, K. W. Köster, A. I. Kolesnikov, V. N. Novikov, R. Richert, R. Bömer, T. Loerting, and A. P. Sokolov, *Proc. Natl. Acad. Sci.*, 2014, **111** 17402-17407.

(21) V. N. Novikov and A. P. Sokolov, *Phys. Rev. Lett.*, 2013, **110**, 065701.

(22) M. Ceriotti, W. Fang, P. G. Kusalik, R. H. McKenzie, A. Michaelides, M. A. Morales, and T. E. Markland, *Chem. Rev.*, 2016, **116**, 7529-7550.

(23) R. T. Hart, Q. Mei, C. J. Benmore, J. C. Neuefeind, J. F. C. Turner, M. Dolgos, B. Tomberli, and P. A. Egelstaff, *J. Chem. Phys.*, 2006, **124**, 134505.

(24) U. Bergmann, D. Nordlund, Ph. Wernet, M. Odelius, L. G. M. Pettersson, and A. Nilsson, *Phys. Rev. B*, 2007, **76**, 024202.

(25) K. H. Kim, H. Pathak, A. S. Perakis, D. Mariedahl, J. A. Sellberg, T. Katayama, Y. Harada, H. Ogasawara, L. G. M. Pettersson, and A. Nilsson, *Phys. Rev. Lett.*, 2017, **119**, 075502.

(26) O. Mishima and H. E. Stanley, *Nature*, 1998, **392**, 164-168.

(27) O. Mishima, *Phys. Rev. Lett.*, 2000, **85**, 334.

(28) V. E. Fortov, R. I. Ilkaev, V. A. Arinin, V. V. Burtzev, V. A. Golubev, I. L. Iosilevskiy, V. V. Khrustalev, A. L. Mikhailov, M. A. Mochalov, V. Y. Ternovoi, and M. V. Zhernokletov, *Phys. Rev. Lett.*, 2007, **99**, 185001.

(29) V. Dzyabura, M. Zaghoo, and I. F. Silvera, *Proc. Natl. Acad. Sci. USA*, 2013, **110**, 8040-8044.

(30) S. Scandolo, *Proc. Natl. Acad. Sci. USA*, 2003, **100**, 3051-3053.

(31) S. A. Bonev, B. Militzer, and G. Galli, *Phys. Rev. B*, 2004, **69**, 014101.

(32) I. Tamblyn and S. Bonev, *Phys. Rev. Lett.*, 2010, **104**, 065702.

(33) R. Li, J. Chen, Xi. Li, E. Wang, and L. Xu, *New J. Phys.*, 2013, **17**, 063023.

(34) M. A. Morales, J. M. McMahon, C. Pierleoni, and D. M. Ceperley, *Phys. Rev. Lett.*, 2013, **110**, 065702.

(35) B. Bernu and D. M. Ceperley, *Path Integral Monte Carlo*, published in *Quantum Simulations of Complex Many-Body Systems: From Theory to Algorithms*, Lecture Notes, J. Grotendorst, D. Marx, A. Maramatsu (Eds.), John von Neumann Institute for Computing, Jülich, NIC Series, Vol **10**, ISBN 3-00-009057-6, pp. 51-61 (2002).

(36) J. Y. Abraham, S. V. Buldyrev, and N. Giovambattista, *J. Phys. Chem. B*, 2011, **115**, 14229-14239.

(37) G. Sun, L. Xu, and N. Giovambattista, *J. Chem. Phys.*, 2017, **146**, 014503.

(38) F. Smallenburg and F. Sciortino, *Phys. Rev. Lett.*, 2015, **115**, 015701.

(39) Y. Liu, J. C. Palmer, A. Z. Panagiotopoulos, and P. G. Debenedetti, *J. Chem. Phys.*, 2012, **137**, 214505.

(40) P. H. Poole, R. K. Bowles, I. Saika-Voivod, and F. Sciortino, *J. Chem. Phys.*, 2013, **138**, 034505.

(41) J. C. Palmer, F. Martelli, Y. Liu, R. Car, A. Z. Panagiotopoulos, and P. G. Debenedetti, *Nature*, 2014, **510**, 385-388.

(42) R. S. Singh, J. W. Biddle, P. G. Debenedetti, and M. A. Anisimov, *J. Chem. Phys.*, 2016, **144**, 144504.

(43) J. W. Biddle, R. S. Singh, E. M. Sparano, F. Ricci, M. A. González, C. Valeriani, J. F. L. Abascal, P. G. Debenedetti, M. A. Anisimov, and F. Caupin, *J. Chem. Phys.*, 2017, **146**, 034502.

(44) T. Sumi and H. Sekino, *RSC Adv.*, 2013, **3**, 12743.

(45) S. Reisman and N. Giovambattista, *J. Chem. Phys.*, 2013, **138**, 064509.

(46) A. Gordon and N. Giovambattista, *Phys. Rev. Lett.*, 2014, **112**, 145701.

(47) F. Reif, *Fundamentals of Statistical and Thermal Physics*, page 246 (Waveland Press, Inc., Long Grove, 2009).

(48) M. A. Morales, C. Pierleoni, E. Schewegler, and D. M. Ceperly, *Proc. Natl. Acad. Sci. USA*, 2010, **107**, 12799-12803.

(49) Z. Yan, S. V. Buldyrev, P. Kumar, N. Giovambattista, and H. E. Stanley, *Phys. Rev. E*, 2008, **77**, 042201.

(50) P. J. Steinhardt, D. R. Nelson, and M. Ronchetti, *Phys. Rev. B*, 1983, **28**, 784.

(51) J. R. Errington and P. G. Debenedetti, *Nature*, 2001, **409**, 318.

(52) S. V. Buldyrev, G. Malescio, C. A. Angell, N. Giovambattista, S. Prestipino, F. Saija, H. E. Stanley, and L. Xu, *J. Phys.: Condens. Matter*, 2009, **21**, 504106.

(53) G. Sun, N. Giovambattista, and L. Xu, *J. Chem. Phys*, 2016, **143**, 244503.

(54) H. M. Gibson and N. B. Wilding, *Phys. Rev. E*, 2006, **73**, 061507.

(55) F. Ricci and P. G. Debenedetti, *J. Chem. Sci.*, 2017, **129**, 801.

(56) J. Luo, L. Xu, C. A. Angell, H. E. Stanley, and S. V. Buldyrev, *J. Chem. Phys.*, 2015, **142**, 224501.

(57) D. A. McQuarrie, *Statistical Mechanics* (University Science Books, Sausalito, CA, USA, 2000).

(58) M. Dzugutov, *Nature*, 1996, **381**, 137.

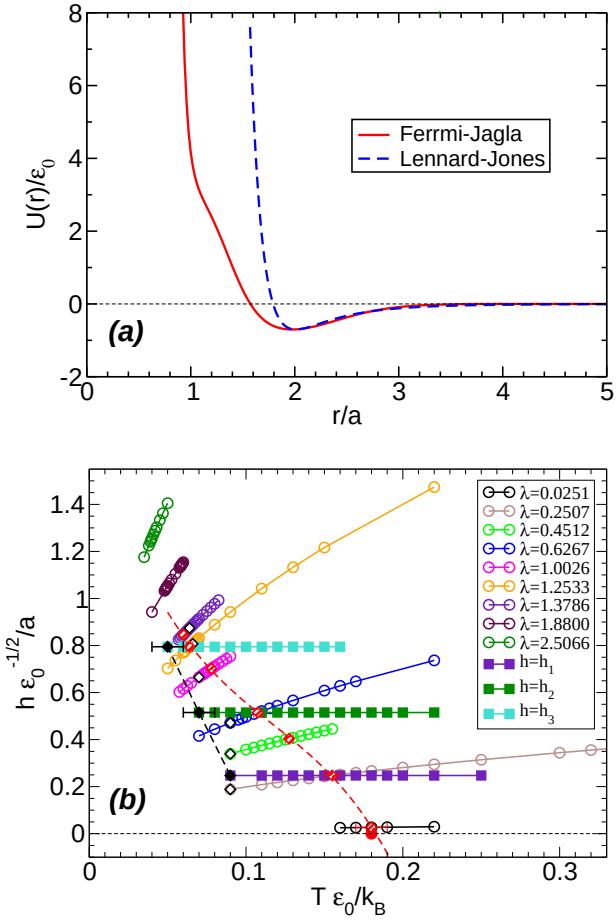

Figure 1: (a) FJ pair interaction potential compared to a Lennard-Jones pair potential with same minimum depth and location. The FJ potential is characterized by a hard-core radius $r \approx a$, a core-softened part at approximately $a \leq r \leq b \approx 2a$, and a weak attractive part. (b)Values of Planck's constant h and temperature T considered in this work. For each point (h, T), we perform a set of constant-(N, v, T) PIMC simulations with $v = 2.0, 2.2, ...4.0$. Simulations are performed along constant-h (filled squares) and constant-λ (empty circles) paths; see text. The red dashed-line indicates the LLCP temperature, $T_c(h)$, for quantum FJ liquids at different values of h. The crystallization temperature $T_x(h)$ for volumes in the range $3.0 < v \leq 3.2$ and for $h = h_1,\ h_2,\ h_3$ is also indicated (black dashed-line and solid diamonds; for comparison, the crystallization temperature along constant-λ paths at $v = 3.2$ is indicated by empty diamonds). Both the $T_c(h)$- and $T_x(h)$-line shift towards lower temperature as h increases, i.e., as the nature of the FJ liquid becomes more quantum, and intersect each other at $h \approx h_3 = 0.7948$. The red solid symbol represents the LLCP for the classical FJ liquid ($h = 0$) reported in Ref.[36]

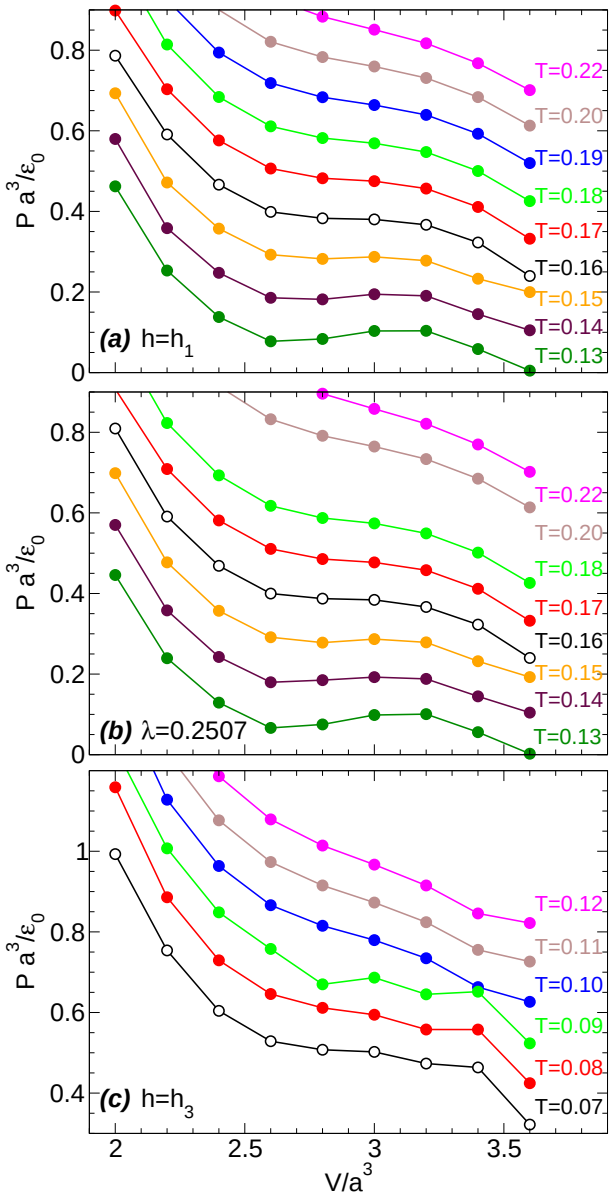

Figure 2: Pressure as function of volume along isotherms for selected constant-h and constant-λ paths in Fig. 1(b): (a) $h = h_1 = 0.2474$, (b) $\lambda = 0.2507$, and (c) $h = h_3 = 0.7948$. The paths in Fig. 1(b) corresponding to (a) and (b) intersect at the LLCP temperature and hence, for these paths, the LLCP occurs at the same conditions: $P_c = 0.38$, $T_c = 0.16$, and $v_c \approx 2.9$. In (c), the LLCP occurs at $P_c \approx 0.50$, $T_c = 0.07$, and $v_c \approx 2.9$, and crystallization occurs at approximately $T < T_c$ (crystallization is also observed at $T = 0.09$ for $v = 2.8,\ 3.2$, at all temperatures for $v = 3.6$, and at $T \leq 0.09$ for $v = 3.4$). For clarity, in (a) and (b), isotherms at $T = 0.17,\ 0.18,\ 0.19,\ 0.20,\ 0.22$ are shifted by $\Delta P = 0.1\ , 0.2,\ 0.3,\ 0.4,\ 0.5$, respectively, while isotherms at $T = 0.15,\ 0.14,\ 0.13$ are shifted by $\Delta P = -0.1, -0.2, -0.3$, respectively; the critical isotherm (empty circles) is not shifted. Similarly, in (c), isotherms at $T = 0.08,\ 0.09,\ 0.10,\ 0.11,\ 0.12$ are shifted by $\Delta P = 0.1\ , 0.2,\ 0.3,\ 0.4,\ 0.5$, respectively.

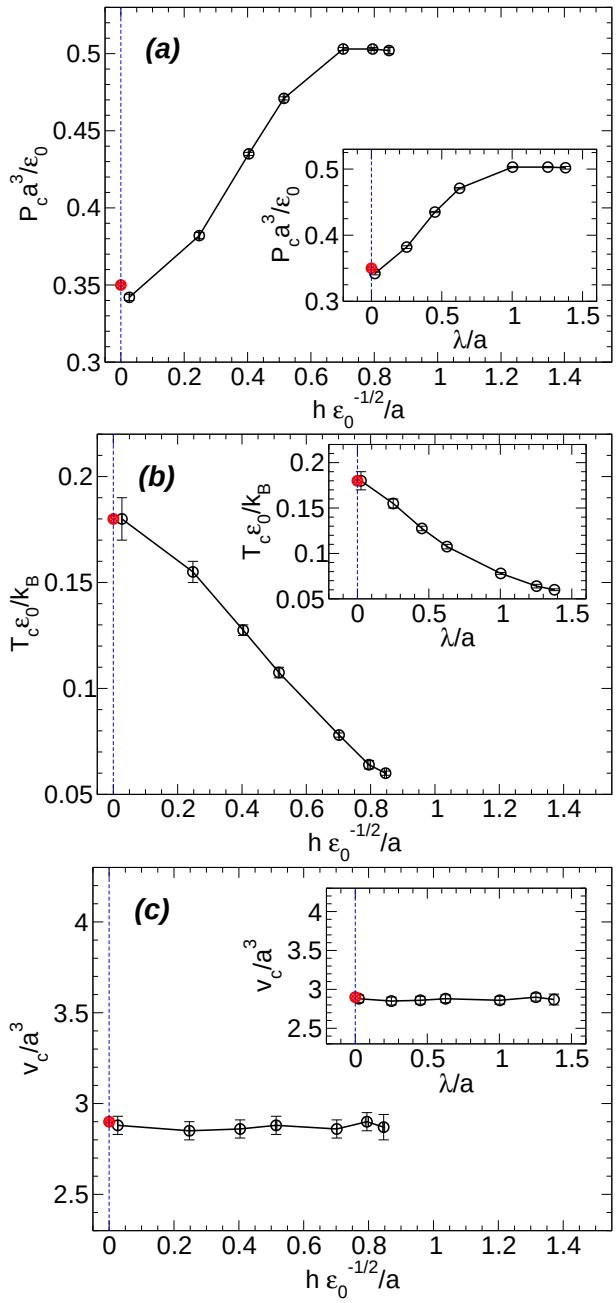

Figure 3: (a) LLCP pressure P_c, (b) temperature T_c, and (c) volume per particle v_c as function of the Planck's constant h. As the quantum character of the liquid increases (i.e., h increases), the LLCP shifts towards higher pressures and lower temperatures, while the critical volume remains unchanged. For approximately $h > h_3 = 0.7948$ ($\lambda = 1.3786$), the LLCP becomes inaccessible due to rapid crystallization. The insets show P_c, T_c, and v_c as function of λ. The red circle indicates the estimated ($P_c,\ T_c,\ v_c$) for the classical FJ liquid ($h = 0$) from Ref.[36]

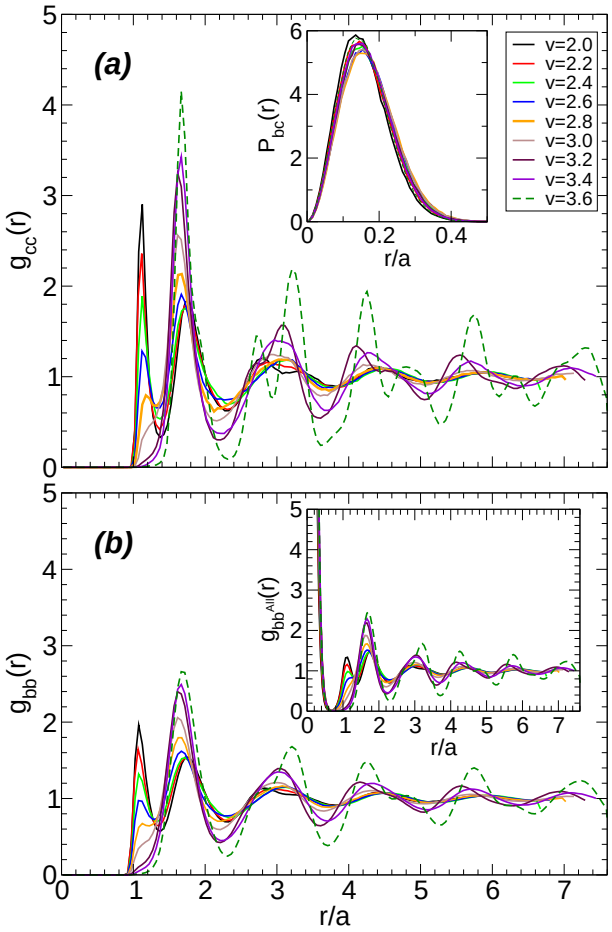

Figure 4: (a) Centroid-centroid RDF for the quantum FJ liquid at $h = h_3$ and $T = T_c(h_3)$, and for different volumes. As the liquid evolves from the LDL-like ($v > v_c \approx 2.9$) to the HDL-like ($v < v_c$) state, the peak of $g_{cc}(r)$ at $r/a \approx 1.7$ decreases while an extra peak develops at $r/a \approx 1$, consistent with structural changes found in the classical FJ liquid ($h = 0$) at $T < T_c$.[36] The system crystallizes at $v = 3.6$. The inset shows the probability distribution $P_{bc}(r)$ to find a bead of a given ring polymer (atom) at a distance r from the corresponding centroid. $P_{bc}(r)$ varies weakly with v and is non-zero up to $r/a \approx 0.4$ indicating that atoms for the FJ liquid at $h = h_3$ are delocalized, expanding up to a distance of ≈ 0.4 times the hard-core radius of the FJ potential. (b) RDF between beads n and m of different ring-polymers (atoms). The main panel shows the case $n = m$, i.e., for interacting beads (statistics is performed over all $n = 1,\ 2,\ 3..., n_b$ beads). The inset corresponds to the case where beads n and m are not necessarily identical ($n, m = 1,\ 2,\ 3..., n_b$). All bead-bead and centroid-centroid RDFs show a similar behavior with increasing v.

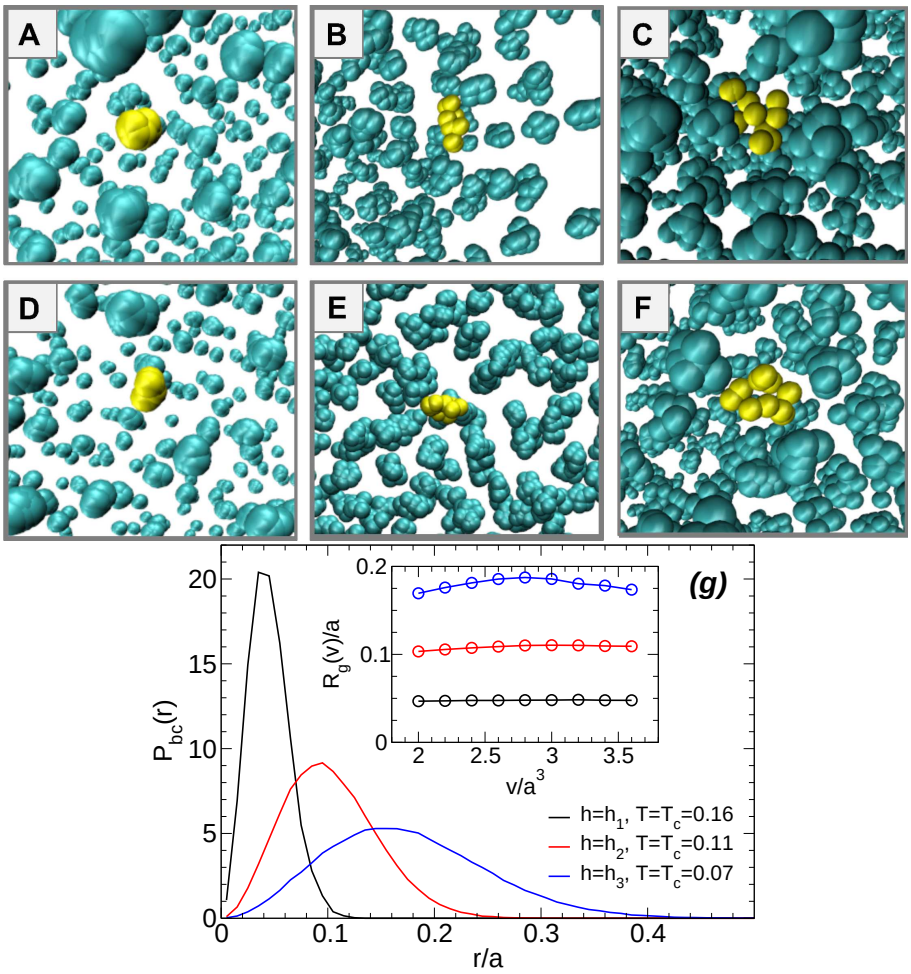

Figure 5: Snapshots showing a typical particle (ring polymer) in (a)(b)(c) HDL at $v = 2.4$ and (d)(e)(f) LDL at $v = 3.4$. Left, middle, and right row correspond, respectively, to quantum FJ liquids with $h = h_1$ and $T = T_c(h_1) = 0.155$, $h = h_2$ and $T = T_c(h_2) = 0.107$, and $h = h_3$ and $T = T_c(h_3) = 0.064$. At the corresponding critical temperature, particles become more delocalized as the quantum nature of the liquid increases (left to right). (g) Probability to find a bead of a ring-polymer (atom) at a distance r from the corresponding centroid for quantum FJ liquids with different values of Planck's constant. All distributions are for $v = 2.8$ and show minor changes with volume. Inset: Average radius of gyration as function of volume for $h = h_1, h_2, h_3$, at the corresponding $T_c(h)$.

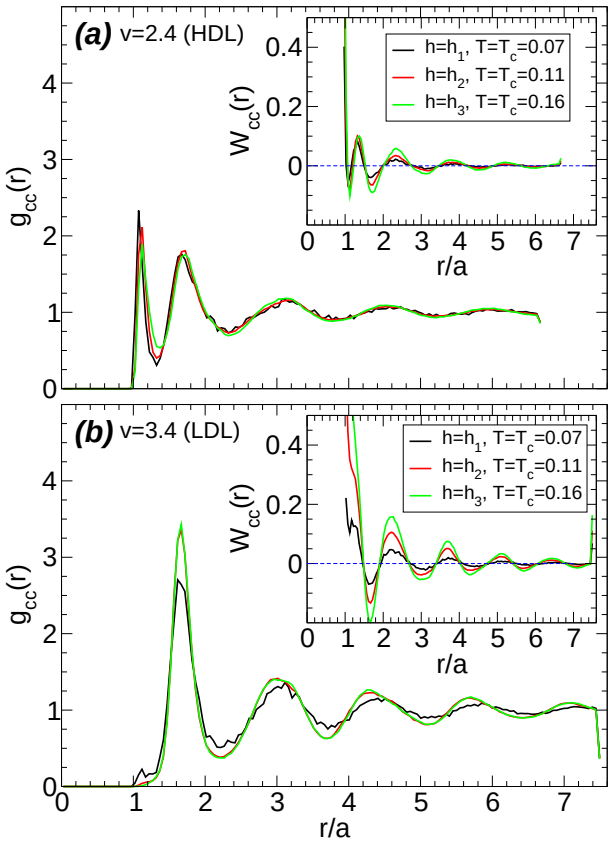

Figure 6: Centroid-centroid RDF for the quantum FJ liquids at $h = h_1,\ h_2,\ h_3$ and $T = T_c(h)$. (a) HDL at $v = 2.4$ and (b) LDL at $v = 3.4$. The relative location of the ring polymers (atoms) centroids in HDL is barely affected by increasing the quantumness (i.e., h) of the system. Similar conclusions seem to hold for LDL (note that the RDF for LDL at $h = h_1$ is rather noisy). Insets: Potential of mean force between centroids in LDL and HDL obtained from the corresponding RDFs in the main panels.

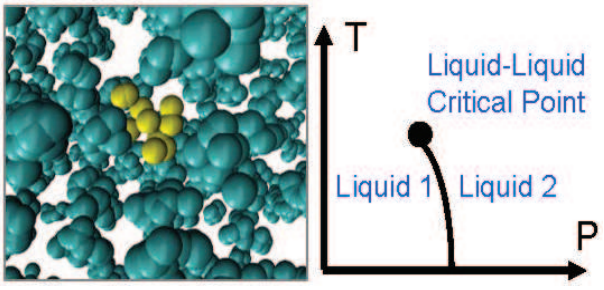

Figure 7: TOC: The liquid-liquid phase transition of a classical monatomic liquid shifts towards low-temperatures and high-pressures when nuclear quantum effects are included.

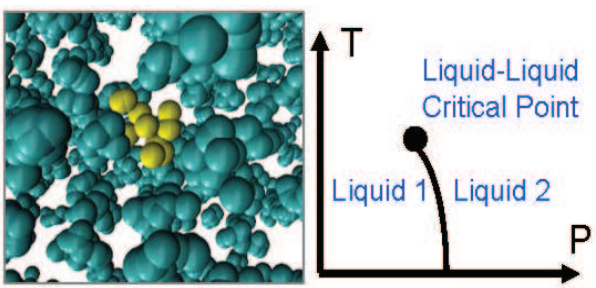
T
Liquid-Liquid
Critical Point
Liquid 1
Liquid 2
P